Enhancing the Performance of Solid-State Dye-Sensitized Solar Cells Using a Mesoporous Interfacial Titania Layer with a Bragg Stack

Jung Tae Park, Jacob H. Prosser, Sung Hoon Ahn, Sang Jin Kim, Jong Hak Kim, and Daeyeon Lee**

High efficiency dye-sensitized solar cells (DSSCs) are fabricated with a heterostructured photoanode that consists of a 500-nm-thick organized mesoporous TiO_2 (om-TiO_2) interfacial layer (IF layer), a 7 or 10-μm thick nanocrystalline TiO_2 layer (NC layer), and a 2-μm-thick mesoporous Bragg stack (meso-BS layer) as the bottom, middle and top layers, respectively. An om-TiO_2 layer with a high porosity, transmittance, and interconnectivity is prepared via a sol-gel process, in which a poly(vinyl chloride)-*g*-poly(oxyethylene methacrylate) (PVC-*g*-POEM) graft copolymer is used as a structure-directing agent. The meso-BS layer with large pores is prepared via alternating deposition of om-TiO_2 and colloidal SiO_2 (col-SiO_2) layers. Structure and optical properties (refractive index) of the om-TiO_2 and meso-BS layers are studied and the morphology of the heterostructured photoanode is characterized. DSSCs fabricated with the heterostructured IF/NC/BS photoanode and combined with a polymerized ionic liquid (PIL) exhibit an energy conversion efficiencies of 6.6% at 100 mW/cm^2, one of the highest reported for solid-state DSSCs and much larger than cells prepared with only a IF/NC layer (6.0%) or a NC layer (4.5%). Improvements in energy conversion efficiency are attributed to the combination of improved light harvesting, decreased resistance at the electrode/electrolyte interface, and excellent electrolyte infiltration.

1. Introduction

Since the pioneering work of the Gratzel group in 1991,[1] TiO_2 nanoparticle-based dye-sensitized solar cells (DSSCs) have become an attractive photovoltaic technology as an alternative to conventional silicon solar cells due to their low cost, high energy conversion efficiency, simple fabrication process, and minimal environmental impact.[2,3] To date, the highest light-to-electric conversion efficiency of 11–12% has been obtained by using a ruthenium polypyridyl complex as the light absorber, an I^-/I_3^- redox couple as the liquid electrolyte, porous titanium dioxide nanocrystal as the photoanode deposited on a transparent conducting oxide (TCO) glass, and a platinum (Pt) coated TCO glass as the counter electrode.[4,5] Research efforts to enhance the conversion efficiency have been focused mainly on the development of efficient dye sensitizers,[6,7] electrolyte,[8–10] nanocrystalline TiO_2 layer,[11,12] counterelectrode,[13,14] or the 3D nanostructured photoanode.[15,16]

The electrolyte is a critical element in determining the photovoltaic performance and stability of DSSCs. Usually, liquid organic solvents such as acetonitrile and methoxy propionitrile have been used as a carrier for I^-/I_3^- redox couples. Although DSSCs with common liquid electrolytes have been reported to show high cell efficiency, there are practical problems such as leakage or evaporation of the solvent, which may reduce the long-term stability of DSSCs. To overcome these drawbacks, several attempts have been made to substitute liquid electrolytes with solidified or quasi-solid-state polymer electrolyte[17–20] and solid-state hole transport materials[21–23] to fabricate solid-state DSSCs (ssDSSCs). Recently, light-to-electric conversion efficiency of 8.5% has been reached in ssDSSCs with $CsSnI_3$ perovskite as a hole-conductor.[24] One of the key considerations in fabricating ssDSSCs is to enable thorough infiltration of high molecular weight electrolytes into the photoanode, which tends to depend on the electrode pore size.

Despite recent progress with incorporating solid electrolytes, there have not been extensive efforts to enhance the device performance of ssDSSCs by modifying non-electrolyte components of the devices such as electrodes. Most studies have focused on improving the long-term stability of devices by optimizing the composition of solid electrolytes. For example, ssDSSC with organic crystal electrolytes were shown to have cell efficiencies of about 4.8%.[25] Such a cell efficiency, however, is significantly

J. T. Park, J. H. Prosser, D. Lee
Department of Chemical and Biomolecular Engineering
University of Pennsylvania
220 South 33rd Street, Philadelphia, PA 19104, USA
E-mail: daeyeon@seas.upenn.edu
J. T. Park, S. H. Ahn, S. J. Kim, J. H. Kim
Department of Chemical and Biomolecular Engineering
Yonsei University
262 Seongsanno, Seodaemun-gu, Seoul 120-749, South Korea
E-mail: jonghak@yonsei.ac.kr

DOI: 10.1002/adfm.201202345

© 2013 WILEY-VCH Verlag GmbH & Co. KGaA, Weinheim

lower than that of DSSCs made with common liquid electrolyte systems. For future applications such as building integrated photovoltaics (BIPV), ssDSSCs with enhanced photovoltaic performance, as well as long-term stability need to be developed.

One approach to enhance the light harvesting efficiency is the introduction of optical elements such as a submicrometer-thick interfacial layer between the micron-thick nanocrystalline TiO_2 layer and the TCO glass.[27,28] Kim et al. recently showed that a mesoporous TiO_2 interfacial layer templated by poly(vinyl chloride)-*g*-poly(oxyethylene methacrylate) (PVC-*g*-POEM) graft copolymer can be deposited with high uniformity and reproducibility for the fabrication of ssDSSCs.[28,29] This interfacial layer results in an increased transmittance of visible light, enhanced electron transfer and better adhesion on the TCO layer, leading to increases in all photovoltaic performance metrics including photocurrent density (J_{sc}), photovoltage (V_{oc}), fill factor (*FF*), and overall conversion efficiency (η).

Another approach to enhance the light harvesting efficiency is to incorporate a photonic crystal layer such as a Bragg reflector into the photoanode structure. The photonic crystal layer reflects non-absorbed photons back to the photoanode, resulting in improved light harvesting. In particular, photoelectrochemical devices with enhanced optical and transport properties have been reported using multilayers.[30,31] Recently, the Hagfeldt and Míguez groups developed a TiO_2 photoanode coupled with a 1D photonic crystal multilayer and reported energy conversion efficiencies (5–7% at 100 mW/cm^2 for liquid electrolyte) much greater than those without photonic crystals.[32,33] In particular, enhancement in the device efficiency using highly porous 1D photonic crystal structure integrated in DSSCs was demonstrated without any compromise in the FF, suggesting that liquid electrolyte penetrated thoroughly into the photoanode.[33] However, small pore size, low porosity, and insufficient pore connectivity of the photonic crystal layer could hinder the solid state electrolyte infiltration into the entire photoanode structure.

In particular, such structures would significantly limit the performance of solid-state DSSCs that utilize high molecular weight polymer electrolytes. The Tetreault group reported the utilization of 3D photonic crystal multilayers on the mesoporous TiO_2 underlayer based on the inverted opal structures of polystyrene particle assemblies; however, the efficiency was low (≈2%) due to a low surface area.[34] Therefore, it is highly desirable to design a strategy to enlarge the pore size without compromising the surface area in the photonic crystal layers in order to enhance the infiltration of high molecular weight solid electrolytes within the TiO_2 photoanode. Recently, the Steiner group presented an effective fabrication route for mesoporous Bragg reflectors based on the self assembly of poly(isoprene-*block*-ethylene oxide) (PI-*b*-PEO) block copolymer in combination with simple hydrolytic sol-gel chemistry, but the solar cell applications were not reported.[35]

In this work, we report the fabrication of heterostructured photoanodes comprising an organized mesoporous TiO_2 (om-TiO_2) interfacial (IF) layer, a nanocrystalline (NC) TiO_2 layer, and a mesoporous Bragg stack (meso-BS) layer as the bottom, middle, and top layers, respectively. The om-TiO_2 layer is prepared via a sol-gel process using a PVC-*g*-POEM graft copolymer template. A graft copolymer is more attractive than a block copolymer due to its low cost and the ease with which it can be synthesized.[12,28,29] The meso-BS layer is prepared by alternating depositions of the om-TiO_2 layer and a colloidal SiO_2 (col-SiO_2) layer. Detailed properties of heterostructures are systematically characterized using spectroscopic ellipsometry, field emission-scanning electron microscopy (FE-SEM), grazing incidence small-angle X-ray scattering (GISAXS), and diffuse reflectance spectra. The DSSCs are fabricated using three electrolytes, i.e. two types of conventional liquid electrolyte and a solid-state polymerized ionic liquid (PIL), and their performance is characterized using current–voltage (*J*–*V*) curves and incident photon to current conversion efficiency (IPCE) spectra. Our results show that ssDSSCs generated with a om-TiO_2 interfacial layer and a meso-BS layer has a conversion efficiency of 6.6%, which is one of the highest values reported to date, which is comparable to that of DSSCs using a common liquid electrolyte.

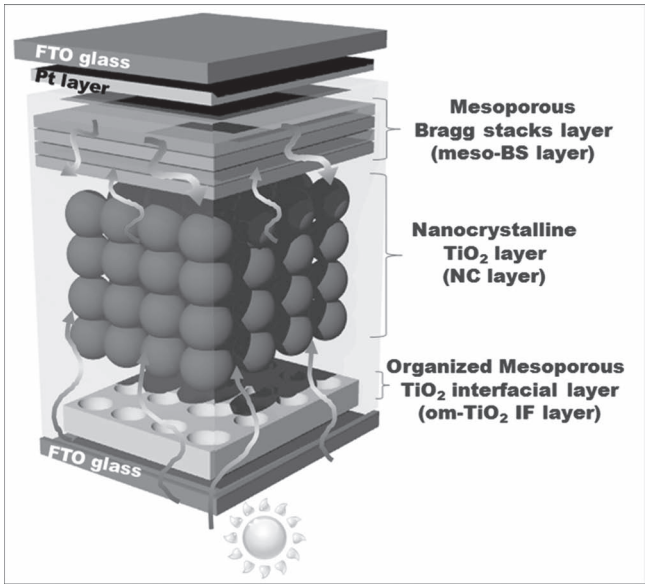

Scheme 1. Structure of DSSCs with the multilayered photoelectrode.

2. Results and Discussion

Our heterostructured photoanode, hypothesized to maximize light harvesting in DSSCs, consists of a 500-nm-thick om-TiO_2 IF layer, a 7-μm (or 10-μm) thick NC layer, and a 2-μm-thick meso-BS layer as the bottom, middle, and top layers, respectively, as shown in **Scheme 1**. The thickness of each layer can be controlled by using a spin-coating method for the om-TiO_2 IF and meso-BS layers, and a doctor blade method for the NC TiO_2 layer. To test the importance of organized mesoporous TiO_2 interfacial layer and mesoporous Bragg Stack in DSSCs, three types of heterostructured photoanodes (NC, IF/NC and IF/NC/BS layer systems) were also prepared.

To enable the formation of mesoporous Bragg stacks as well as the om-TiO_2 interfacial layer, we first characterized the structure and properties of a om-TiO_2 film and a col-SiO_2 film,

© 2013 WILEY-VCH Verlag GmbH & Co. KGaA, Weinheim

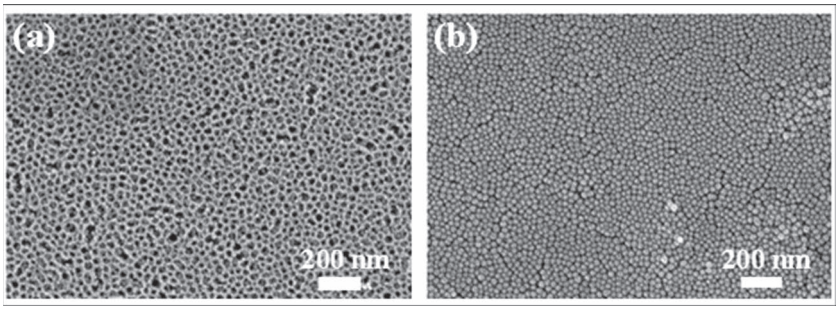

Figure 1. FE-SEM images of a) plan-view of om-TiO_2 and b) plan-view of col-SiO_2.

which were used as the high and low refractive index layers of Bragg stacks, respectively. The refractive indices at 632.8 nm of the om-TiO_2 interfacial and col-SiO_2 layer were determined to be 1.71 and 1.30 using ellipsometry, respectively. In the case of the mesoporous TiO_2 layer, a well-organized structure with a high porosity, uniform pores, and good interconnectivity was obtained as seen in the plan-view SEM image of om-TiO_2 film (**Figure 1**a). The confinement of precursor, TTIP to the hydrophilic POEM domains of the PVC-*g*-POEM graft copolymer and its conversion to TiO_2 nanocrystals upon calcination results in the observed structure. This layer was utilized as the high index layer of the Bragg stacks as well as the interfacial layer between the TCO and the TiO_2 NC layer. Also, plan-view SEM images confirmed that the heterostructured photoanodes layer depositions did not perturb the mesoporous structure of om-TiO_2 films significantly (Supporting Information Figure S1). As for the col-SiO_2 layer, a randomly packed structure with interstitial voids between nanoparticles is observed, as shown in Figure 1b. Previous studies have shown that the pore size in randomly packed colloidal films tend to be comparable to the size of the constituent particles.[36] Thus, we believe the pore size in the colloidal SiO_2 layer is around 20–30 nm, similar to the pore size in the mesoporous TiO_2 layer. The large pores present in the TiO_2 and SiO_2 layers composing the Bragg stacks would open the opportunity to achieve better pore-filling of high molecular weight electrolytes while maintaining the high reflectance properties for an improved light harvesting efficiency.

Using the mesoporous TiO_2 and colloidal SiO_2 layers characterized above, heterostructured photoanodes were assembled based on the design illustrated in Scheme 1. The structure and optical property of the photoanode after deposition of each layer on a pristine fluorine-doped tin oxide (FTO) glass was characterized using photography, scanning electron microscopy (SEM), and UV-visible spectroscopy. The deposition of om-TiO_2 IF layer on an FTO glass resulted in an increase in light transmittance in the visible region as shown in **Figure 2**. The photoanode with 7-μm (or 10-μm) thick NC TiO_2 layer, deposited using the doctor blade method, was opaque, whereas the photoanode with a 2-μm-thick meso-BS layer a top the NC TiO_2 layer showed characteristic iridescence (Figure 2a), suggesting the formation of a photonic structure. The microstructure of the heterostructured photoanode was further characterized by cross-sectional SEM as shown in Figure 2b–d. The meso-BS layer atop the NC TiO_2 layer is composed of om-TiO_2 layers and col-SiO_2 nanoparticle layers with the periodicity of approximately 200 nm. The interfaces between the two layers are sharp and smooth as seen in Figure 2b. The thicknesses of the high and low index regions were controlled to generate a Bragg stack that has one of its higher order reflectance peaks around 450 nm. The use of a higher order peak has shown to be a reliable method to achieve strong Bragg reflection even if the thickness of each layer in the stack is slightly different from the ideal values.[37,38] In detail, the thickness and refractive index of each dielectric layer in the meso-BS layer gives rise to optical interference effects that result in the Bragg diffraction peak position. However, meso-BS based on thin layers to achieve UV or violet-blue region reflectance may also lead to a greater possibility of an imperfection structure because it needs very precise thickness control.[37] Therefore, one solution to realize a high quality meso-BS layer that has UV or violet-blue region reflectance is through the use of high order Bragg diffraction. In addition, a bi-functional BS layer with undermost thick om-TiO_2 layer deposited onto the NC layer acts as a highly efficient reflector and also as a dye adsorbable active layer, which can improve the light harvesting efficiency. The cross-sectional image of the heterostructured photoanode near the FTO glass

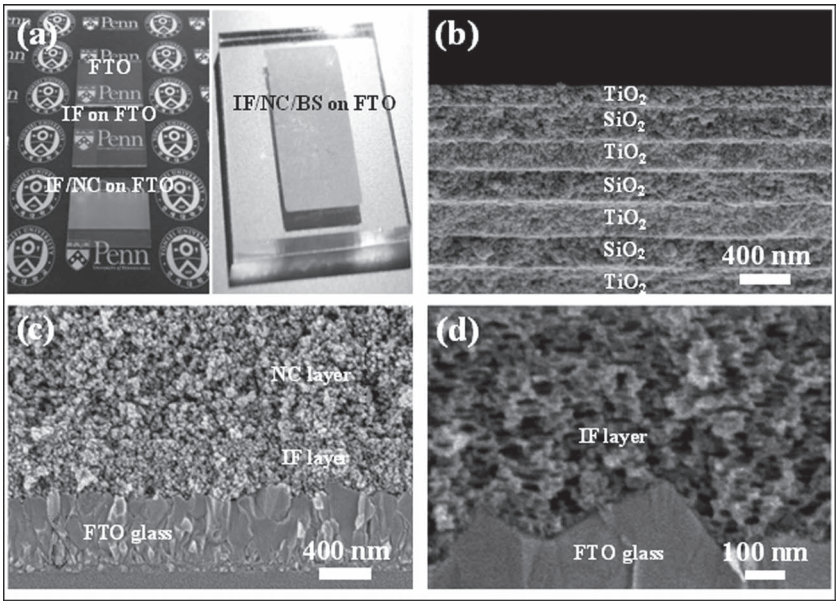

Figure 2. a) Photographs of pristine FTO glass, IF layer on FTO, IF/NC layer on FTO and IF/NC/BS layer on FTO glass, b) cross-section of meso-BS layer consisting of om-TiO_2 and col-SiO_2, c) cross-section of IF/NC layer on FTO, and d) magnified cross-section of IF layer on FTO.

© 2013 WILEY-VCH Verlag GmbH & Co. KGaA, Weinheim

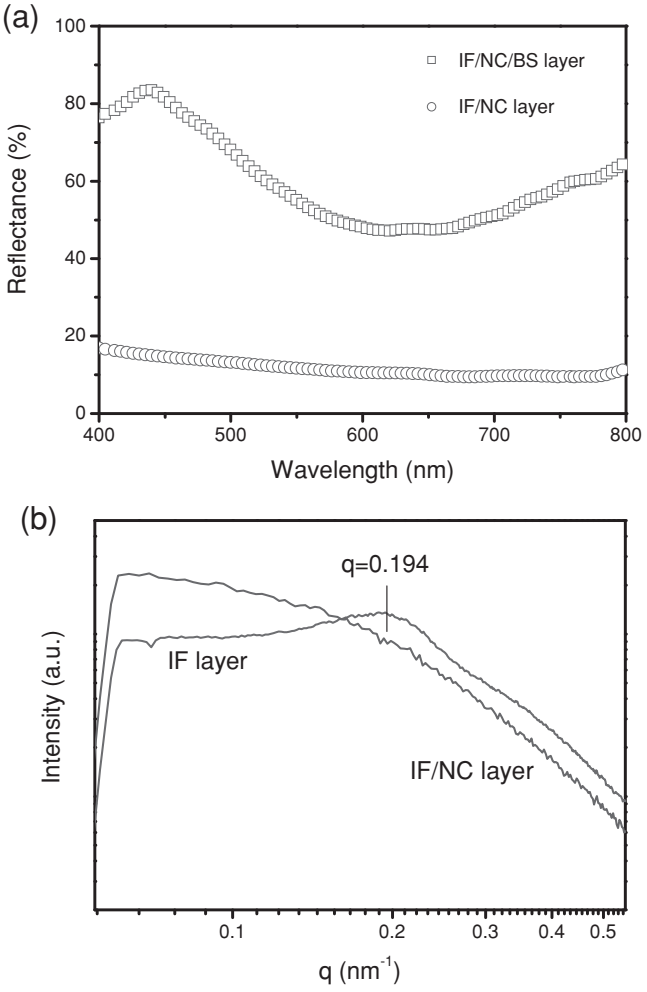

Figure 3. a) Reflectance spectra of IF/NC and IF/NC/BS layers on FTO glass and b) GISAXS spectra of IF and IF/NC layers on FTO glass.

shows a mesoporous structure and a well-defined interface between the IF and NC layers (Figure 2c). The magnified image of the om-TiO_2 layer/FTO interface (Figure 2d) reveals that an organized mesoporous structure with a high porosity and excellent interconnectivity is also present in all directions, and the om-TiO_2 layer is conformally adhered to the FTO substrate without any defects such as delamination or cracks. Our previous study has shown that the formation of the IF layer decreases the effective roughness of the FTO from 8.4 to 3.2 nm and, in turn, improves the transmittance of visible light by suppressing roughness enhanced scattering.[29] Excellent interfacial contact between the FTO and the om-TiO_2 layer also leads to facile electron transport through the photoanode, leading to the suppression of the back recombination process.[28]

The reflectance spectra of TiO_2 photoanodes with different structures were characterized to investigate the effect of the meso-BS layer on the optical properties of the photoanode, as shown in **Figure 3**a. The reflectance of the IF/NC/BS photoanode was approximately 50–85% in the range of 400–800 nm, which is much greater than that (9–16%) for a photoanode with only a IF/NC layer and no BS. This result suggests that a significant fraction of incident light was redirected by the meso-BS layer, which could lead to an increased utilization of solar light in DSSCs. A typical Bragg stack, commonly known as a photonic reflector, shows high transparency without a diffuse scattering feature outside the reflectance band. The Bragg stack generated in our photoanode design, in contrast, shows significant scattering outside of the reflectance band. Similar structures with thick dielectric layers in the Bragg stack to enhance scattering in addition to reflection have also been demonstrated very recently.[39] In addition, previous studies have shown that such a reflective or diffuse scattering layer can enhance the efficiency of DSSCs by allowing more light to scatter back to the inner cell.[40,41] Therefore, the Bragg stack utilized in our study provides enhanced reflection as well as diffuse scattering, and, at the same time, also presents relatively large pores, which we believe would lead to better light harvesting efficiency and improved infiltration of the electrolytes into the TiO_2 nanopores. The reflection peak of the IF/NC/BS photoanode without electrolyte was located at the violet, blue-colored visible region (≈450 nm). Previous DSSCs studies have shown that the highest cell performance enhancements were obtained when the reflectance band of the photonic layers in the absence of the electrolyte was observed in the violet region. The infiltration of the electrolyte into the photoanode was shown to red shift the reflectance band to a longer wavelength that is close to the absorption band of the sensitizer such as N719 dye.[42]

The structure of the om-TiO_2 layer was also characterized using grazing incidence small-angle X-ray scattering (GISAXS). A broad scattering peak at around $q = 0.194$ nm was observed in the om-TiO_2 IF layer indicating its well-ordered regularity over a large area, as shown in Figure 3b. Using the relation $d = 2\pi/q$, the d-spacing was determined to be 32.4 nm, which is consistent with the average pore size (20–30 nm) of the om-TiO_2 IF layer, as determined by SEM image analysis. However, this scattering peak completely disappeared upon the deposition of NC layer over the IF layer due to the random structure of the NC layer that dominates the scattering properties of the structure.

The ssDSSCs were fabricated with different photoanode structures (i.e., with NC only, IF/NC and IF/NC/BS layers) in which the thickness of the NC layer was approximately 7 μm. The corresponding J–V curves of each structure were determined under simulated sunlight radiation of 100 mW/cm^2, as shown in **Figure 4**a. The photovoltaic performances of these ssDSSCs are summarized in **Table 1**. We used polymerized ionic liquid (PIL), poly(1-((4 ethenylphenyl)methyl)-3-butylimidazolium iodide) (PEBII) as a solid electrolyte because this material has been previously shown to generate ssDSSCs with high performance and stability.[23] The ssDSSC with 7-μm-thick NC layer exhibited an energy conversion efficiency of 3.5%, which is comparable to ssDSSCs that have been presented in other reports.[23,25] However, the introduction of om-TiO_2 IF layer between the FTO and the NC layer increased the conversion efficiency of the solar cell to 5.4%. The high cell efficiency is due to the enhanced transmittance of visible light into the photoanode, suppression of the back recombination of electrons at the interface between the FTO electrode and the electrolyte, and improved interfacial properties between the FTO glass and the TiO_2 layer, resulting in the increase of the J_{sc}, V_{oc}, and FF value.[27,28,43]

© 2013 WILEY-VCH Verlag GmbH & Co. KGaA, Weinheim

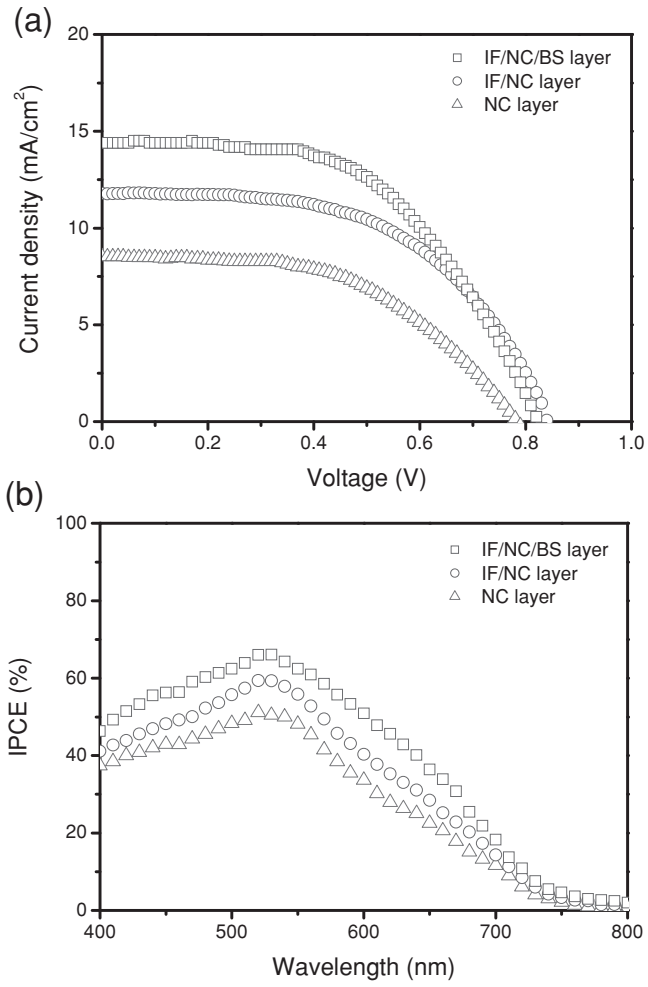

Figure 4. a) *J–V* curves and b) IPCE values of the ssDSSCs assembled with three types of photoelectrode deposited on a FTO substrate and PIL as a solid electrolyte at 100 mW/cm^2. The thickness of NC layer is approximately 7 μm.

When the photoanode was prepared with a meso-BS as the top layer, the J_{sc} value was further increased from 11.8 to 14.4 mA/cm^2, whereas the V_{oc} and *FF* values were only slightly reduced, resulting in further improvement of the efficiency to 6.4%. One possible contribution to the improved J_{sc} value is the increased light reflection and scattering effect from the meso-BS layer deposited atop the photoanode. The slight decrease of V_{oc} value is likely due to the SiO_2 in the meso-BS layer, which is an insulator that increases the rate of the recombination process at negative biases.[44] The slight decrease in FF may be due to the structure of the meso-BS layer, which does not fully allow for the deep infiltration of solid PIL electrolyte into the TiO_2 photoanode. Similar results were obtained in the DSSCs fabricated when two different types of liquid electrolytes were used, as shown in Supporting Information Figure S2 and **Table 2**,**3**.

Light harvesting efficiency of DSSCs was also investigated by IPCE values, as shown in Figure 4b. Considering similar electron injection and electron collection efficiencies among the cells, the improved IPCE values are most likely due to an enhancement in the light harvesting efficiency, leading to increasing J_{sc} values.[45] The introduction of om-TiO_2 IF layer resulted in the increase of the IPCE values over the 400–800 nm wavelength range due to the increased transmittance of visible light, indicating an improved light harvesting efficiency. The IPCE value of the cell with the IF/NC/BS heterostructured photoanode was significantly greater than those with the IF/NC or only the NC layer, demonstrating that the meso-BS layer plays an important role as an effective photonic layer to enhance reflecting unabsorbed photons back into the photoanode. Therefore, the heterostructured photoanodes were able to enhance the light harvesting properties based on the improved transmittance of visible light due to the interfacial layer and the redirection of incident light due to the Bragg stack layer.

We were also able to further enhance the efficiency of the DSSCs by increasing the thickness of the NC layer from 7 to 10 μm, as shown in Supporting Information Figure S3 and **Table 4**. Remarkably, the device efficiency of ssDSSCs using the solid PIL reached 6.6% at 100 mW/cm^2, which is comparable to that of DSSCs with the traditional liquid electrolyte (Type 1) and one of the highest values for ssDSSCs.[23,25,29,46,47] The higher efficiency of ssDSSC is attributed to higher ionic concentration, well-organized structure and lower glass transition

Table 1. Cell performances including V_{oc}, J_{sc}, *FF*, and η for the ssDSSCs fabricated with three types of TiO_2 photoelectrode and solid PIL electrolyte (PEBII poly(1-((4 ethenylphenyl)methyl)-3-butyl-imidazolium iodide)) at 100 mW/cm^2. The thickness of NC layer is approximately 7 μm.

Electrode type	V_{oc} [V]	J_{sc} [mA/cm^2]	*FF*	η [%]
NC	0.79	8.5	0.52	3.5
IF/NC	0.84	11.8	0.55	5.4
IF/NC/BS	0.82	14.4	0.54	6.4

Table 2. Cell performances including V_{oc}, J_{sc}, *FF*, and η for the DSSCs fabricated with three types of TiO_2 photoelectrodes and liquid electrolytes (Type 1: LiI/I_2/TBP in 3-methoxypropionitrile) at 100 mW/cm^2. The thickness of the NC layer is approximately 7 μm.

Electrode type	V_{oc} [V]	J_{sc} [mA/cm^2]	*FF*	η [%]
NC	0.69	9.1	0.60	3.8
IF/NC	0.71	13.0	0.63	5.8
IF/NC/BS	0.71	15.5	0.63	7.0

Table 3. Cell performances including V_{oc}, J_{sc}, FF and efficiency (η) for the DSSCs fabricated with three types of TiO_2 photoelectrodes and liquid electrolytes (Type 2: 1-butyl-3-methylimidazolium iodide/I_2/guanidinium thiocyanate/4-tert-butylpyridine in acetonitrile and valeronitrile) at 100 mW/cm^2. The thickness of the the NC layer is approximately 7 μm.

Electrode Type	V_{oc} [V]	J_{sc} [mA/cm^2]	*FF*	η [%]
NC	0.71	9.3	0.63	4.2
IF/NC	0.72	13.2	0.65	6.2
IF/NC/BS	0.71	15.9	0.65	7.4

© 2013 WILEY-VCH Verlag GmbH & Co. KGaA, Weinheim

Table 4. Cell performances including V_{oc}, J_{sc}, *FF* and η for the DSSCs fabricated with three types of TiO_2 photoelectrodes consisting of 10-μm-thick NC layer at 100 mW/cm^2.

Electrode Type	Electrolyte Type	V_{oc} [V]	J_{sc} [mA/cm^2]	*FF*	η [%]
NC	PIL[a)]	0.63	13.7	0.52	4.5
	L[b)]	0.60	14.1	0.60	4.8
	L[c)]	0.72	14.4	0.64	6.6
IF/NC	PIL[a)]	0.66	16.1	0.56	6.0
	L[b)]	0.64	16.7	0.64	6.2
	L[c)]	0.73	17.0	0.66	8.1
IF/NC/BS	PIL[a)]	0.65	18.3	0.55	6.6
	L[b)]	0.63	18.7	0.64	7.0
	L[c)]	0.72	18.8	0.65	8.8

[a)]Solid electrolyte: poly(1-((4 ethenylphenyl)methyl)-3-butyl-imidazolium iodide)), PEBII; [b)]Liquid electrolyte: (Type 1: LiI/I_2/TBP in 3-methoxypropionitrile.); [c)]Liquid electrolyte: (Type 2: 1-butyl-3-methylimidazolium iodide/I_2/guanidinium thiocyanate/4-tert-butylpyridine in acetonitrile and valeronitrile.)

temperature (T_g) of PEBII.[23] These results indicate that relatively large pores that are present in the BS layer and IF layer enhance the infiltration of high molecular weight PIL electrolyte and thus the device efficiency is in fact very close to that of liquid electrolyte DSSCs. The efficiency of the liquid DSSCs was further improved up to 8.8% at 100 mW/cm^2 by optimizing the composition of the electrolyte (i.e., Type 2 liquid electrolyte), which again illustrates the synergy of incorporating om-TiO_2 and meso-BS layer into the photoanode of the DSSC. In addition, the interfacial resistance at the electrode/electrolyte interface and recombination kinetics of ssDSSCs were also investigated using electrochemical impedance spectroscopy (EIS), and are plotted in Supporting Information Figure S4a and S4b, respectively. All spectra recorded were simulated and plotted using Z plot software with an equivalent circuit that depicts a general transmission line electrical model established originally to describe the macroscopic homogeneous porous electrode model. A smaller interfacial resistance at the electrode/electrolyte interface and a longer electron lifetime of within the IF/NC/BS layers were obtained, indicating sufficient infiltration of solid state PIL electrolyte into the photoanode and suppressed recombination process.[48,49] This likely results from a BS layer with a high porosity and organized mesoporous structure, which allows for enhanced interfacial contact between the electrode and the electrolyte, and more efficient electron transfer.

Also, to verify the advantage of using the BS layer over the commercial scattering layer as light harvesting structures, a ssDSSC system with a commercial scattering (CS) layer was also prepared and the performance characterized, as shown in Supporting Information Figure S5 and Table S1. Upon using solid PIL as the solid electrolyte, the ssDSSC fabricated with a IF/NC/BS photoanode exhibited 6.4% at 100 mW/cm^2, which is significantly greater than the efficiency of the IF/NC/CS photoanode system (5.7%). This is reasonable considering that the bi-functional BS layer with an undermost om-TiO_2 layer allows for reflection as well as the scattering of the unabsorbed photons back into the cell and also provides additional surface area for dye adsorption. Both factors could contribute to enhancing the light harvesting, and therefore, improving the J_{sc} value of ssDSSCs.

3. Conclusion

In summary, we prepared and tested the ssDSSCs incorporating heterostructured photoanodes consisting of a om-TiO_2 IF layer, a NC TiO_2 layer, and a meso-BS layer as the bottom, middle, and top layers, respectively. The meso-BS layer with large pores was prepared via an alternate deposition of om-TiO_2 and col-SiO_2 layers. The DSSCs based on the heterostructured IF/NC/BS photoanodes showed higher efficiency than those with IF/NC or only NC photoanodes. Upon using PIL as a solid electrolyte, an energy conversion efficiency of 6.6% at 100 mW/cm^2 could be achieved, which is one of the highest values reported for ssDSSCs to date. The efficiency improvements resulted from the combination of a well-organized structure of IF layer and meso-BS layer, leading to improved light collection, decreased resistance at electrode/electrolyte interface, and excellent electrolyte infiltration as confirmed by IPCE and reflectance measurements. We believe that the graft copolymer-assembly directed approach introduces a new and cheap route toward the synthesis of well-organized BS layers as an alternative to a conventional block copolymer self-assembly.

4. Experimental Section

Poly(vinyl chloride) (PVC, M_w = 97 000 g mol^{-1}, M_n = 55 000 g mol^{-1}), poly(oxyethylene methacrylate) (POEM, poly(ethylene glycol) methyl ether methacrylate, M_n = 475 g mol^{-1}), 1,1,4,7,10,10-hexamethyltriethylene tetramine (HMTETA, 99%), copper(I) chloride (CuCl, 99%), titanium(IV) isopropoxide (TTIP, 97%), hydrochloric acid (HCl, 37 wt%), LUDOX TM-40 (40 wt% SiO_2 suspension in H_2O, 22 nm), 1-butylimidazole, 4-chloromethylstyrene, lithium iodide (LiI), magnesium sulfate ($MgSO_4$), 2,2′-azobisisobutyronitrile (AIBN), iodine (I_2), 3-methoxypropionitrile, butylmethylimidazolium iodide, guanidinium thiocyanate, 4-tert-butylpyridine, valeronitrile, and chloroplatinic acid hexahydrate (H_2PtCl_6) were purchased from Sigma-Aldrich (St Louis, MO). Tetrahydrofuran (THF), *N*-methyl pyrrolidone (NMP), methanol, 2-propanol, chloroform, acetonitrile, diethylether and ethyl acetate were purchased from J.T. Baker. Deionized water (>18 MΩ m) was obtained with a water purification system made by Millipore Corporation. Ruthenium dye (535-bisTBA, N719), TiO_2 colloidal paste (Ti-Nanoxide, D20), and 60 μm thick Surlyn were purchased from Solaronix, Switzerland. FTO conducting glass substrate (TEC8, 8 ohms/sq, 2.3 mm thick) was purchased from Pilkington, France. All solvents and chemical reagents used in our experiments were obtained from commercial sources as guaranteed grade reagents and used without further purification.

Synthesis of the Graft Copolymer Template (PVC-g-POEM): PVC-*g*-POEM graft copolymer was synthesized via atomic transfer radical polymerization (ATRP) process, according to the previously reported method.[28] In brief, 6 g of PVC was dissolved in 50 mL of NMP by stirring at 90 °C for 4 h. After cooling the solution to room temperature, 15 g of POEM, 0.1 g of CuCl, and 0.23 mL of HMTETA were added to the solution. The green mixture was stirred until producing homogeneous solution, and was purged with nitrogen for 30 min. The reaction was carried out at 90 °C for 18 h. After polymerization, the resultant mixture was diluted with THF. After passing the solution through a column with

© 2013 WILEY-VCH Verlag GmbH & Co. KGaA, Weinheim

activated Al_2O_3 to remove the catalyst, the solution was precipitated into methanol. The grafted copolymer was purified by dissolving in THF and re-precipitating into methanol three times. PVC-*g*-POEM graft copolymer with PVC:POEM = 1:1.5 wt% ratio was obtained in a powder form and dried in a vacuum oven overnight at room temperature.

Preparation of the TiO_2 Sol-Gel Solution Using Graft Copolymer Template: The PVC-*g*-POEM graft copolymer template with a specific weight ratio of 1:1.5 was used as template for the preparation of TiO_2 sol-gel solution. Titanium isopropoxide (TTIP) was used as a precursor for TiO_2. In a typical procedure, 0.05 g of PVC-*g*-POEM graft copolymer was first dissolved in 1.5 mL of THF. Separately, 0.15 mL of concentrated HCl (37 wt%) was slowly added to 0.3 mL of TTIP at room temperature under vigorous stirring. An additional 0.15 mL of DI water was slowly added to the TTIP solution. For this mixture, the volume ratio of [TTIP]:[HCl]:[H_2O] was 2:1:1. After aging for 15 min in room temperature condition, the TTIP solution was slowly added to the PVC-*g*-POEM graft copolymer solution under stirring. This solution was subsequently aged under mild stirring at room temperature for 3 h before film casting.

Preparation of the Aggregated SiO_2 Colloidal Suspensions: Aggregated SiO_2 colloidal suspensions were prepared according to the previously described procedure with a few modifications.[50] In a 30 mL vial, LUDOX TM-40 (40 wt% SiO_2 suspension in H_2O, 22 nm in size) was adjusted to pH 7.0 by using HCl and the solution was aged for 3 h at 60 °C with stirring. This procedure was required to decrease the negative surface charge on the SiO_2 nanoparticles and produce particle aggregation through condensation process of hydroxyl groups (–OH) at the silica surface.

Preparation of Heterostructured Photoanodes: *Formation of IF Layer (Bottom Photoanode Layer)*: Before deposition of the mesoporous IF layer, the FTO glasses were cleaned by isopropanol and chloroform in an ultrasonic bath for 30 min in each case, respectively. Then, as prepared TiO_2 sol-gel solutions were deposited onto the FTO glasses at 1500 rpm for 30 s using a SMSS Delta 80BM spin coater. After spin coating, the films were put into a vacuum oven and treated at 50 °C for 30 min. Finally, the films were subsequently calcined under air by heating at a rate of 3 °C/min to 450 °C, holding for 30 min to remove the organic chemicals and to nucleate and grow TiO_2 nanoparticles in the mesoporous IF layer.

Formation of NC Layer (Middle Photoanode Layer): Before building the SiO_2/TiO_2 BS layer onto the coated substrate, the commercial TiO_2 paste (Ti-Nanoxide D20, Solaronix) was cast onto the mesoporous IF layer coated FTO glass using a doctor-blade technique in order to obtain smooth and uniform film. Then, the IF/NC coated FTO glasses were heated to 450 °C for 30 min in air.

Formation of BS Layer (Top Photoanode Layer): SiO_2/TiO_2 BS layer was prepared using anatase titanium oxide nanoparticles (STS-100, 18 wt% of 7nm TiO_2 suspension in water) and silica nanoparticles (Ludox SM-30, 30 wt% of 7nm SiO_2 suspension in water).[51] In our experiment, the thickness of meso-BS layers was carefully controlled by dilution of the SiO_2 colloidal suspensions and TiO_2 sol-gel solution with water and THF, respectively. For the formation of meso-BS layers, an alternate deposition of SiO_2 (7.61 wt%) nanoparticles solutions and TiO_2 (5.78 wt%) macromolecular templating solutions was performed using spin-coating at 2000 and 1500 rpm, respectively. In between each layer deposition, heat treatment was performed in a furnace at 500 °C for 1 h to remove water bonded to the nanoparticles surface and mechanically stabilize the entire structure. The deposition was repeated until the desired number of layers was obtained.

Dye Adsorption onto Heterostructured TiO_2 Photoanodes: HeterostructuredTiO_2 photoanodes were sensitized with a 0.1 mM ruthenium solution in ethanol at 50 °C for 24 h in a dark room. The dye-sensitized TiO_2 photoanodes were rinsed with 200 proof ethanol and dried in a vacuum oven.

Preparation of Counterelectrodes: Transparent glasses coated with FTO were used for counter electrodes. The glasses were cleaned by sonication in isopropanol and then in chloroform. The counter electrodes were made by spin-coating a drop of 4 wt% solution of H_2PtCl_6 isopropanol solution onto the conductive FTO glass substrate and heated under air flow at 450 °C for 30 min and cooling to 30 °C over 8 h.

Fabrication of DSSCs: Particular attention was paid to three types of electrolytes for the fabrication of DSSCs: 1) solid-state polymerized ionic liquid (PIL), i.e., poly(1-((4 ethenylphenyl)methyl)-3-butyl-imidazolium iodide) (PEBII); 2) Type 1 liquid electrolyte consisting of lithium iodide (LiI), iodine (I_2) and 4-tert-butylpyridine (TBP); and 3) Type 2 liquid electrolyte consisting of 1-butyl-3-methylimidazolium iodide, iodine (I_2), guanidinium thiocyanate, and 4-tert-butylpyridine (TBP) in acetonitrile and valeronitrile. For the ssDSSCs system, a PIL electrolyte solution was prepared by dissolving a PEBII solution (2 and 10 wt%) in acetonitrile. The PIL electrolyte solution deeply infiltrated the photoanode and covered the counter electrode, according to the previously reported procedure.[12,23,28] The cells were placed in a drying oven at 40 °C for 24 h and subsequently in a vacuum oven at 40 °C for 24 h to ensure complete solvent evaporation. Then, the DSSCs were placed in a vacuum oven for a day to permit complete evaporation of the solvent and then sealed with an epoxy resin. In the case of liquid system, the DSSCs with liquid electrolyte were assembled using 60 µm thick Surlyn, then the inner spaces of the DSSCs were filled with a liquid electrolyte solution through a drilled hole on the counter electrode. Type 1 liquid electrolyte solution was composed of 0.5 M LiI, 0.05 M I_2 and 0.5 M TBP in 3-methoxypropionitrile. Type 2 liquid electrolyte was composed of 0.6 M 1-butyl-3-methylimidazolium iodide, 0.03 M I_2, 0.1 M guanidinium thiocyanate, and 0.5 M 4-tert-butylpyridine in a mixture of acetonitrile and valeronitrile (v/v, 85:15).[52] The DSSCs were illuminated with a Keithley Model 2400 and a 1000 W xenon lamp (Oriel, 91193). The light intensity was homogeneous over an 8×8 in^2 area. A correction for the spectral mismatch between the simulated light and natural sunlight was made against a certified reference Si solar cell (Fraunhofer Institute for Solar Energy System, Mono-Si + KG filter, Certificate No. C-ISE269) for a sunlight intensity of one (100 mW/cm^2). This calibration was verified with an NREL-calibrated Si solar cell (PV Measurements Inc.). The DSSCs temperature was maintained at 25 °C throughout the measurement time using peltier cooling apparatus. The photoelectrochemical performances were calculated by the following equations:

$$FF = \frac{V_{max}\, J_{max}}{V_{oc}\; J_{sc}} \tag{1}$$

$$\eta(\%) = \frac{V_{max}\, J_{max}}{P_{in}} \times 100 = \frac{V_{oc}\, J_{sc}\, FF}{P_{in}} \times 100 \tag{2}$$

where J_{sc} is a short-circuit current density (mA/cm^2), V_{oc} is an open-circuit voltage (V), P_{in} is an incident light power, *FF* is the fill factor, η is an overall energy conversion efficiency and J_{max} (mA/cm^2) and V_{max} (V) are the current density and voltage in the *J*–*V* curve, respectively, at the point of maximum power output. The photoanode active area, determined by the aperture of a black mask, was 0.16 cm^2.

The IPCE was measured as a function of wavelength from 400 to 800 nm (K3100) under short circuit conditions using an irradiation of a 300 W xenon lamp, which was obtained by a series of light filters with different wavelengths. The IPCE value was calculated using the following equation:

$$IPCE = \frac{hcI}{\lambda p} \tag{3}$$

where *h* and *c* represent Planck's constant and the speed of light in a vacuum, respectively. *I* is the photocurrent density (mA/cm^2). λ and *P* are the wavelength (nm) and the intensity (mA/cm^2) of the incident monochromatic light, respectively.

Characterization: Thickness and refractive index of mesoporous Bragg Stacks are determined using a spectroscopic ellipsometer, Alpha-SE, and the Complete EASE software package (J.A. Woollam). The images of electrode surface and cross-section were obtained with a field emission-scanning electron microscope with operating at 2 kV (FE-SEM) (SUPRA 55VP, Carl Zeiss). The diffuse reflectance spectra of TiO_2 photoanodes were acquired using UV–visible spectrophotometer (Hewlett- Packard, Hayward, CF) over a sample area of roughly 5×5 µm^2 with a magnification of 100. A spectral range of 400–800 nm was explored using

© 2013 WILEY-VCH Verlag GmbH & Co. KGaA, Weinheim

a tungsten-halogen lamp. The grazing incidence small-X ray scattering (GISAXS) experiments were conducted at the 3C SAXS I beamline at the Pohang Light Source (PLS), Korea. The operating conditions were set to a wavelength of 1.608 Å ($\Delta\lambda/\lambda = 1.5 \times 10^{-2}$) and the sample-to-detector distance of 2 m, the beam size of 1×1 mm^2. The samples were mounted in a vacuum chamber with an incidence angle of 0.20°, which is between the critical angle of the sample and that of the FTO substrate. Electrochemical impedance spectroscopy (EIS) analysis was used to investigate the internal resistance at the electrode/electrolyte interface and the recombination kinetics of TiO_2 photoelectrodes in DSSCs.

Supporting Information

Supporting Information is available from the Wiley Online Library or from the author.

Acknowledgements

This work supported by NSF CBET-1234993, NSF CBET-1033017, NSF DMR-1055594, the Penn MRSEC (DMR-1120901), the Korea Center for Artificial Photosynthesis (KCAP) (NRF-2011-C1AAA001-2011-0030278) and the Pioneer Research Center Program (2008-05103). J.H.P. and J.T.P. acknowledge the support of an NSF-IGERT fellowship (DGE-0221664) and the Yonsei University Research Fund 2012, respectively.

Received: August 16, 2012
Revised: October 17, 2012
Published online: November 22, 2012

[1] B. O'Regan, M. Gratzel, *Nature* **1991**, *353*, 737.
[2] M. Gratzel, *Nature* **2001**, *414*, 338.
[3] L. Schmidt-Mende, U. Bach, R. Humphry-Baker, T. Horiuchi, H. Miura, S. Ito, S. Uchida, M. Gratzel, *Adv. Mater.* **2005**, *17*, 813.
[4] F. Gao, Y. Wang, D. Shi, J. Zhang, M. Wang, X. Jing, R. Humphry-Baker, P. Wang, S. M. Zakeeruddin, M. Gratzel, *J. Am. Chem. Soc.* **2008**, *130*, 10720.
[5] C. Y. Chen, M. K. Wang, J. Y. Li, N. Pootrakulchote, L. Alibabaei, C. H. Ngoc-Le, J. D. Decoppet, J. H. Tsai, C. Gratzel, C. G. Wu, S. M. Zakeeruddin, M. Gratzel, *ACS Nano* **2009**, *3*, 3103.
[6] C. Y. Chen, J. G. Chen, S. J. Wu, J. Y. Li, C. G. Wu, K. C. Ho, *Angew. Chem. Int. Ed.* **2008**, *47*, 7342.
[7] A. Yella, H.-W. Lee, H. N. Tsao, C. Yi, A. K. Chandiran, M. K. Nazeeruddin, E. W.-G. Diau, C.-Y. Yeh, S. M. Zakeeruddin, M. Gratzel, *Science* **2011**, *334*, 629.
[8] H. J. Snaith, A. J. Moule, C. Klein, K. Meerholz, R. H. Friend, M. Gratzel, *Nano Lett.* **2007**, *7*, 3372.
[9] N. Cai, S.-J. Moon, L. Cevey-Ha, T. Moehl, R. Humphry-Baker, P. Wang, S. M. Zakeeruddin, M. Gratzel, *Nano Lett.* **2011**, *11*, 1452.
[10] K. S. Lee, Y. Jun, J. H. Park, *Nano Lett.* **2012**, *12*, 2233.
[11] J. Wu, Y. Xiao, Q. Tang, G. Yue, J. Lin, M. Huang, Y. Huang, L. Fan, Z. Lan, S. Yin, T. Sato, *Adv. Mater.* **2012**, *24*, 1884.
[12] S. H. Ahn, W. S. Chi, J. T. Park, J. K. Koh, D. K. Roh, J. H. Kim, *Adv. Mater.* **2012**, *24*, 519.
[13] S. I. Cha, B. K. Koo, S. H. Seo, D. Y. Lee, *J. Mater. Chem.* **2010**, *20*, 659.
[14] Q. Tai, B. Chen, F. Guo, S. Xu, H. Hu, B. Sebo, X.-Z. Zhao, *ACS Nano* **2011**, *5*, 3795.
[15] N. Tetreault, E. Arsenault, L.-P. Heiniger, N. Soheilnia, J. Brillet, T. Moehl, S. Zakeeruddin, G. A. Ozin, M. Gratzel, *Nano Lett.* **2011**, *11*, 4579.
[16] H. K. Yu, W. J. Dong, G. H. Jung, J.-L. Lee, *ACS Nano* **2011**, *5*, 8026.
[17] H. X. Wang, H. Li, B. F. Xue, Z. X. Wang, Q. B. Meng, L. Q. Chen, *J. Am. Chem. Soc.* **2005**, *127*, 6394.
[18] O. Winther-Jensen, V. Armel, M. Forsyth, D. MacFarlane, *Macromol. Rapid Commun.* **2010**, *31*, 479.
[19] M. Wang, X. Pan, X. Fang, L. Guo, W. Liu, C. Zhang, Y. Huang, L. Hu, S. Dai, *Adv. Mater.* **2010**, *22*, 5526.
[20] Z. Lan, J. Wu, S. Hao, J. Lin, M. Huang, Y. Huang, *Energy Environ. Sci.* **2009**, *2*, 524.
[21] T. Leijtens, I.-K. Ding, T. Giovenzana, J. T. Bloking, M. D. McGehee, A. Sellinger, *ACS Nano* **2012**, *6*, 1455.
[22] I. Y. Song, S.-H. Park, J. Lim, Y. S. Kwon, T. Park, *Chem. Commun.* **2011**, *47*, 10395.
[23] W. S. Chi, J. K. Koh, S. H. Ahn, J.-S. Shin, H. Ahn, D. Y. Ryu, J. H. Kim, *Electrochem. Commun.* **2011**, *13*, 1349.
[24] I. Chung, B. Lee, J. He, R. P. H. Chang, M. G. Kanatzidis, *Nature* **2012**, *485*, 486.
[25] Q. Li, X. Chen, J. Zhao, L. Qiu, Y. Zhang, B. Sun, Feng Yan, *J. Mater. Chem.* **2012**, *22*, 6674.
[26] C.-H. Lee, W.-H. Chiu, K.-M. Lee, W.-F. Hsieh, J.-M. Wu, *J. Mater. Chem.* **2011**, *21*, 5114.
[27] Y. J. Kim, Y. H. Lee, M. H. Lee, H. J. Kim, J. H. Pan, G. I. Lim, Y. S. Choi, K. Kim, N.-G. Park, C. Lee, W. I. Lee, *Langmuir* **2008**, *24*, 13225.
[28] S. H. Ahn, H. Jeon, K. J. Son, H. Ahn, W.-G. Koh, D. Y. Ryu, J. H. Kim, *J. Mater. Chem.* **2011**, *21*, 1772.
[29] J. Kim, J. K. Koh, B. Kim, S. H. Ahn, H. Ahn, D. Y. Ryu, J. H. Kim, E. Kim, *Adv. Funct. Mater.* **2011**, *21*, 4633.
[30] N. Tetreault, M. Gratzel, *Energy Environ. Sci.* **2012**, *5*, 8506.
[31] C. Lopez-Lopez, S. Colodrero, S. R. Raga, H. Lindstrom, F. Fabregat-Santiago, J. Bisquertb, H. Miguez, *J. Mater. Chem.* **2012**, *22*, 1751.
[32] S. Colodrero, A. Mihi, L. Haggman, M. Ocana, G. Boschloo, A. Hagfeldt, H. Miguez, *Adv. Mater.* **2009**, *21*, 764.
[33] S. Colodrero, A. Forneli, C. Lopez-Lopez, L. Pelleja, H. Miguez, E. Palomares, *Adv. Funct. Mater.* **2012**, *22*, 1303.
[34] S. Guldin, S. H. ttner, M. Kolle, M. E. Welland, P. Muller-Buschbaum, R. H. Friend, U. Steiner, N. Tetreault, *Nano Lett.* **2010**, *10*, 2303.
[35] S. Guldin, M. Kolle, M. Stefik, R. Langford, D. Eder, U. Wiesner, U. Steiner, *Adv. Mater.* **2011**, *23*, 3664.
[36] M. I. Dafinone, G. Feng, T. Brugarolas, K. E. Tettey, D. Lee, *ACS Nano* **2011**, *5*, 5078.
[37] O. Sanchez-Sobrado, M. E. Calvo, H. Mıguez, *J. Mater. Chem.* **2010**, *20*, 8240.
[38] S. Y. Choi, M. Mamak, G. V. Freymann, N. Chopra, G. A. Ozin, *Nano Lett.* **2006**, *6*, 2456.
[39] D. Colonna, S. Colodrero, H. Lindstrom, A. D. Carlo, H. Miguez, *Energy Environ. Sci.* **2012**, *5*, 8238.
[40] M. E. Calvo, S. Colodrero, N. Hidalgo, G. Lozano, C. Lopez-Lopez, O. Sanchez-Sobrado, H. Miguez, *Energy Environ. Sci.* **2011**, *4*, 4800.
[41] T. T. T. Pham, T. Bessho, N. Mathews, S. M. Zakeeruddin, Y. M. Lam, S. Mhaisalkar, M. Gratzel, *J. Mater. Chem.* **2012**, *22*, 16201.
[42] C. T. Yip, H. Huang, L. Zhou, K. Xie, Y. Wang, T. Feng, J. Li, W. Y. Tam, *Adv. Mater.* **2011**, *23*, 5624.
[43] A. J. Frank, N. Kopidakis, J. V. D. Lagemaat, *Coord. Chem. Rev.* **2004**, *248*, 1165.
[44] E. Palomares, J. N. Clifford, S. A. Haque, T. Lutz, J. R. Durrant, *J. Am. Chem. Soc.* **2003**, *125*, 475.
[45] K. Zhu, N. R. Neale, A. Miedaner, A. J. Frank, *Nano Lett.* **2007**, *7*, 69.
[46] J. Xia, N. Masaki, M. Lira-Cantu, Y. Kim, K. Jiang, S. Yanagida, *J. Am. Chem. Soc.* **2008**, *130*, 1258.
[47] S. Nejati, K. K. S. Lau, *Nano Lett.* **2011**, *11*, 419.
[48] J. Burschka, V. Brault, S. Ahmad, L. Breau, M. K. Nazeeruddin, B. Marsan, S. M. Zakeeruddin, M. Gratzel, *Energy Environ. Sci.* **2012**, *5*, 6089.
[49] J. T. Park, W. S. Chi, D. K. Roh, S. H. Ahn, J. H. Kim, *Adv. Funct. Mater.* **2012**, DOI: 10.1002/adfm.201200823.
[50] K. T. Cook, K. Tettey, R. M. Bunch, D. Lee, A. J. Nolte, unpublished.
[51] D. Lee, M. F. Rubner, R. E. Cohen, *Nano Lett.* **2006**, *6*, 2305.
[52] J. T. Park, R. Patel, H. Jeon, D. J. Kim, J.-S. Shin, J. H. Kim, *J. Mater. Chem.* **2012**, *22*, 6131.

© 2013 WILEY-VCH Verlag GmbH & Co. KGaA, Weinheim